Progress In Electromagnetics Research, PIER 103, 285–303, 2010

ELECTROMAGNETIC WAVE PROPAGATION IN CHIRAL H-GUIDES

A. L. Topa, C. R. Paiva, and A. M. Barbosa

Instituto de Telecomunicações
Department of Electrical and Computer Engineering
Instituto Superior Técnico
Av. Rovisco Pais 1, 1049-001 Lisboa, Portugal

Abstract—Guided-wave propagation in chiral H-guides is analyzed, using a building-block approach. In a first stage, a 2D chiral parallel-plate waveguide is studied using a lossless frequency dispersion model for the optically active medium, where the constitutive chiral parameter is assumed to be dependent on the gyrotropic parameter. In the second stage, the mode matching technique and the transverse resonance method are used to characterize the 3D structure. A full parametric study is presented for a fixed frequency. The operational and dispersion diagrams for the chiral H-guide are presented. By replacing the common isotropic slab with a chiral slab, chirality provides an extra degree of freedom in the design of new devices.

1. INTRODUCTION

Chiral media are known to exhibit optical activity, while keeping reciprocity. Therefore, unlike magnetically biased ferrites, these media can be useful in the design of some reciprocal devices such as mode converters, polarizers and phase shifters (see [1] and references therein). The application of chiral media to closed metallic waveguides, originally termed as chirowaveguides, and to open slab waveguides and circular rods has been exhaustively studied in the last years [2–14]. However, to the authors' best knowledge, no work has been published yet on their application to hybrid waveguides as an H-guide. The major reason for this may be the unfeasibility of an exact closed solution for any rectangular geometry waveguide, due to the coupled differential equations that govern the transverse variation of the field

Corresponding author: A. L. Topa (antonio.topa@lx.it.pt).

components. In fact, TE and TM modes cannot propagate whenever metallic rectangular cross-section waveguiding structures are filled with chiral materials. Some numerical analyses have been presented in the literature for the metallic rectangular waveguide totally filled with a chiral material [2–4], based on the finite-element or finite-difference methods. Exact analytical solutions are only available for the metallic circular waveguide [2], for a ground chiral slab [5], and for the parallel-plate waveguide [6–10], totally or partially filled. The analysis of isotropic-chiral material discontinuities in rectangular waveguides, using the coupled mode method combined with the mode matching technique, has been presented in [11]. The same approach has been used for the analysis of a parallel-plate waveguide partially filled with a chiral media [12]. On the other hand, for very small values of the chirality parameter χ, the solutions to the modal equation can be expressed in terms of this parameter up to first order [13, 14], the zero order term being the solutions for the achiral waveguide and the first order term, which is proportional to χ, would give the impact of chirality on the solution. With this approach, it is possible to grant insight into the transition from TE/TM modes, in the achiral case, to hybrid modes in the chiral case. But this approach is limited to geometries for which an analytical solution of the modal equation can be derived.

This paper addresses the guided-wave propagation in an H-guide when the common isotropic slab is replaced by a chiral slab (Fig. 1). The main advantage of H-guides is the possibility of frequency scaling. Therefore, devices based on chiral waveguides, operating in the microwave regime [1], can be realized at higher frequencies (e.g., in the millimeter-wave regime) using chiral H-guides.

Several examples of H-guides, involving other types of complex media, have been already published in the literature, namely, the

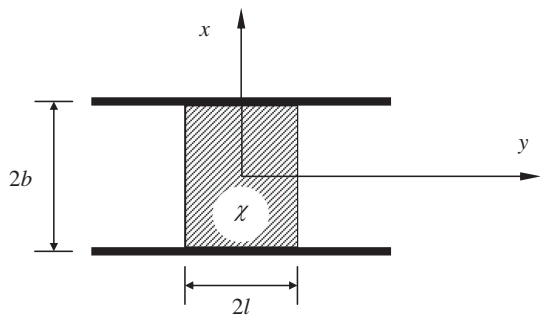

Figure 1. Chiral H-guide.

cases when the isotropic slab is replaced by a uniaxial crystal [15], a transversely magnetized ferrite [16], an omega medium [17] or a double-negative metamaterial [18]. However, so far, no analysis has been published for the chiral H-guide. This can be an interesting structure as chirality may provide an important degree of freedom and allow new potential applications.

A semi-analytical method, based on a building-block approach, is used in this paper. When compared with fully numerical methods (like the finite-element method), this approach allows more physical insight into the results. The procedure is based on the transverse resonance method together with a mode matching technique, as an extension of the method used in [19, 20], after the method originally derived by Peng and Oliner [21]. The building-block approach is divided in two stages. In a first stage, a chiral parallel-plate waveguide is studied using a frequency dispersion model for the optically active medium. When operating at lower frequencies, far below the resonance frequency of the chiral particles, losses may be neglected and dispersion may be characterized by the simple Condon model. A constitutive chiral parameter based on the gyrotropic parameter is assumed [22]. This study provides the elementary modes propagating in the inner region, which are then used for the complete full-wave analysis. Several numerical results for the chiral H-guide are presented in the last section.

2. THE CHIRAL PARALLEL-PLATE WAVEGUIDE

The parallel-plate waveguide is the elementary constitutive 2D structure of an H-guide. In this Section, we analyze the chiral parallel-plate waveguide depicted in Fig. 2. Since this is a completely closed structure, with perfectly conducting planes placed at $x = \pm b$, only discrete modes may propagate.

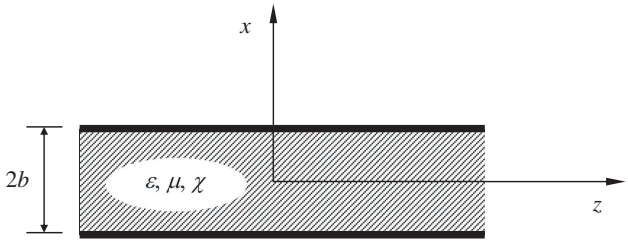

Figure 2. Chiral parallel-plate waveguide.

2.1. Chiral Media

For a chiral medium, the constitutive relations may be written as

$$\begin{bmatrix} \mathbf{D} \\ \mathbf{B} \end{bmatrix} = \begin{bmatrix} \varepsilon_0\varepsilon & -j\sqrt{\varepsilon_0\mu_0}\chi \\ j\sqrt{\varepsilon_0\mu_0}\chi & \mu_0\mu \end{bmatrix} \begin{bmatrix} \mathbf{E} \\ \mathbf{H} \end{bmatrix} \tag{1}$$

with $\varepsilon_0 Z_0 = \mu_0 Y_0 = \sqrt{\varepsilon_0\mu_0} = 1/c$, where c is the vacuum light velocity and χ is the normalized chirality parameter, which can be modeled by $\chi(\omega) = cg\omega$, where g is the gyrotropy parameter. The chirality parameter, responsible for the optical activity and spatial dispersion, is an odd function of frequency and vanishes in the steady-state regime.

Considering plane wave propagation of the form $\exp[-j(kz - \omega t)]$, and using Maxwell's equations for source-free regions in the frequency domain

$$\begin{bmatrix} \nabla\times\mathbf{I} & \mathbf{0} \\ \mathbf{0} & -\nabla\times\mathbf{I} \end{bmatrix} \begin{bmatrix} \mathbf{E} \\ \mathbf{H} \end{bmatrix} = -j\omega \begin{bmatrix} \mathbf{B} \\ \mathbf{D} \end{bmatrix} \tag{2}$$

where $\mathbf{I}$ is the unit dyadic, we can easily see that, in unbounded chiral media, there are two TEM characteristic waves: a RCP (right-hand circularly polarized) wave and a LCP (left-hand circularly polarized) wave and hence, in optically active media, the polarization plane of linearly polarized light rotates with propagation.

Using now Bohren's decomposition [23], one may write

$$\mathbf{D}_\pm = \varepsilon_0\varepsilon_\pm\mathbf{E}_\pm \tag{3}$$

$$\mathbf{B}_\pm = \mu_0\mu_\pm\mathbf{H} \tag{4}$$

where $\varepsilon_\pm = \varepsilon \pm y_c\chi$ and $\mu_\pm = \mu \pm \chi/y_c$ with $y_c = Y_c/Y_0 = \sqrt{\varepsilon/\mu}$. Therefore, Maxwell Equation (2) are recast into

$$\nabla\times\mathbf{E}_\pm = -j\omega\mu_0\mu_\pm\mathbf{H}_\pm \tag{5}$$

$$\nabla\times\mathbf{H}_\pm = j\omega\varepsilon_0\varepsilon_\pm\mathbf{E}_\pm \tag{6}$$

Choosing E_y and H_y as the field supporting components

$$E_y(x,y,z,t) = F(x)\exp[-j(kz - \omega t)] \tag{7}$$

$$H_y(x,y,z,t) = G(x)\exp[-j(kz - \omega t)] \tag{8}$$

the other field components may be obtained from (5) and (6) according to

$$E_x^\pm = \frac{k}{\omega\varepsilon_0\varepsilon_\pm}H_y^\pm \tag{9}$$

$$E_z^\pm = -\frac{j}{\omega\varepsilon_0\varepsilon_\pm}\frac{\partial H_y^\pm}{\partial x} \tag{10}$$

$$H_x^\pm = -\frac{k}{\omega\mu_0\mu_\pm}E_y^\pm \tag{11}$$

$$H_z^{\pm} = \frac{j}{\omega\mu_0\mu_{\pm}} \frac{\partial E_y^{\pm}}{\partial x} \tag{12}$$

while $E_y^{\pm}$ satisfy to the Helmholtz equation

$$\nabla^2 E_y^{\pm} + k_{\pm}^2 E_y^{\pm} = 0 \tag{13}$$

with $k_{\pm} = (\sqrt{\varepsilon\mu} \pm \chi)k_0 = \varepsilon_{\pm}k_0/y_c = y_c\mu_{\pm}k_0$. According to Bohren's decomposition,

$$E_y = E_y^+ + E_y^- \tag{14}$$

$$H_y = H_y^+ + H_y^- = jY_c(E_y^+ - E_y^-) \tag{15}$$

Writing

$$E_y^{\pm} = \Psi_{\pm}(x) \exp\left[-j(kz - \omega t)\right] \tag{16}$$

one has

$$F(x) = \Psi_+(x) + \Psi_-(x) \tag{17}$$

$$G(x) = jY_c\left[\Psi_+(x) - \Psi_-(x)\right] \tag{18}$$

where, according to (13), $\Psi_{\pm}(x)$ obey to the following Helmholtz equation

$$\nabla^2\Psi_{\pm} + (k_{\pm}^2 - k^2)\Psi_{\pm} = 0 \tag{19}$$

Owing to the symmetry of the structure, the propagating modes can be divided into even and odd modes. Therefore, the solutions of (19) can be written as

$$\Psi_{\pm} = A_{\pm}\cos(h_{\pm}x) \tag{20}$$

for the even modes, and

$$\Psi_{\pm} = A_{\pm}\sin(h_{\pm}x) \tag{21}$$

for the odd modes, where $h_{\pm}^2 = k_{\pm}^2 - k^2$.

2.2. Dispersion Diagram

Due to the perfectly conducting planes, placed at $x = \pm b$, one must have $E_y(x = \pm b) = 0$ and $E_z(x = \pm b) = 0$. Imposing these boundary conditions to the six field components derived in Appendix A, a homogeneous set of algebraic equations, for the coefficients $A_{\pm}$ in (20) and (21), is obtained. For a nontrivial solution, the determinant of the correspondent matrix must be zero, leading to the following two modal equations

$$\frac{\varepsilon_-h_+ + \varepsilon_+h_-}{2}\sin\left[(h_+ + h_-)b\right] \pm \frac{\varepsilon_-h_+ - \varepsilon_+h_-}{2}\sin\left[(h_+ - h_-)b\right] = 0. \tag{22}$$

where the plus sign stands for the even modes and the minus sign for the odd modes,

At the cutoff, one has $k = 0$ or, according to (19), $h_{\pm} = k_{\pm}$. At this point, one can use $\varepsilon_- h_+ = \varepsilon_+ h_-$ in the modal Equations (22), to obtain $\sin[(k_+ + k_-)b] = 0$, or $b/\lambda = n/(4\sqrt{\varepsilon\mu})$, with n being an integer. The fundamental even mode, with no cutoff frequency, is obtained for $n = 0$.

The dispersion diagram for the first even and odd hybrid modes is depicted in Fig. 3, for $\varepsilon = 4$, $\mu = 1$, $b = 0.001\,\mathrm{m}$ and $g = 10^{-21}\,\mathrm{s}^2/\mathrm{m}$. The two dashed oblique lines in this figure correspond to the asymptotic limiting values of $k = k_+$ and $k = k_-$. For all modes, k goes to k_+ when $b/\lambda \to \infty$, although transiently they may approach k_-. Moreover, except for the fundamental mode, all dispersion curves start at the cutoff for $k = 0$. One should note that the cutoff values of the odd modes are exactly the same as for the even modes.

This diagram is very important as it provides the numerical values for the wavenumbers of the elementary modes propagating obliquely along the chiral slab of the H-guide. These values are necessary in the mode matching technique applied to the transverse resonance method, as it will be discussed in the next section.

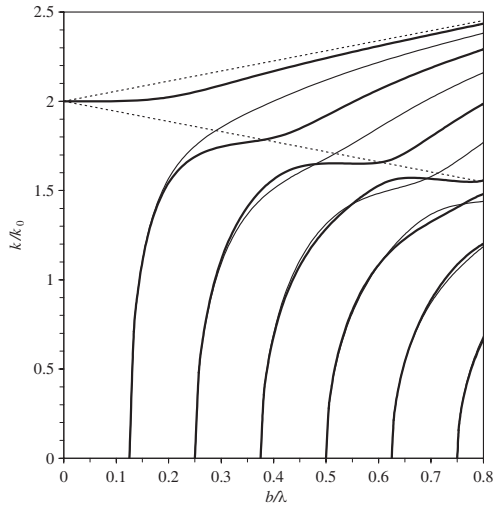

Figure 3. Dispersion diagram for the first propagating modes of a chiral parallel-plate waveguide, with $\varepsilon = 4$, $\mu = 1$, $b = 0.001\,\mathrm{m}$ and $g = 10^{-21}\,\mathrm{s}^2/\mathrm{m}$: (a) Even modes (thick lines); (b) Odd modes (thin lines).

3. THE CHIRAL STEP DISCONTINUITY

3.1. Scattering Matrix under Oblique Incidence

In this section, the step discontinuity in a parallel-plate waveguide depicted in Fig. 4 is analyzed and its scattering matrix under oblique incidence is derived. The mathematical framework presented in this section is quite different from the formalism used in [19, 20], where the elementary modes were pure TE and TM modes, and the waveguide under consideration was a completely open structure. In fact, the modal propagation along the chiral H-guide can be seen as the transverse resonance of the elementary hybrid modes of a parallel-plate waveguide propagating obliquely and bouncing back and forth at two lateral step discontinuities.

The structure coordinates (x, y, z) and the wave coordinates (x, u, v) can be simply related through

$$\begin{bmatrix} x \\ y \\ z \end{bmatrix} = \begin{bmatrix} 1 & 0 & 0 \\ 0 & \sin\theta & \cos\theta \\ 0 & -\cos\theta & \sin\theta \end{bmatrix} \begin{bmatrix} x \\ u \\ v \end{bmatrix} \tag{23}$$

For an incident mode, one has

$$\begin{cases} \mathbf{k}^i = \beta \mathbf{v} \\ \mathbf{E}^i = \{E_x \hat{\mathbf{x}} + E_u \hat{\mathbf{u}} + E_v \hat{\mathbf{v}}\} \exp(-j\beta v) \\ \mathbf{H}^i = \{H_x \hat{\mathbf{x}} + H_u \hat{\mathbf{u}} + H_v \hat{\mathbf{v}}\} \exp(-j\beta v) \end{cases} \tag{24}$$

where

$$\begin{cases} \hat{\mathbf{u}} = \sin\theta\, \hat{\mathbf{y}} - \cos\theta\, \hat{\mathbf{z}} \\ \hat{\mathbf{v}} = \cos\theta\, \hat{\mathbf{y}} + \sin\theta\, \hat{\mathbf{z}} \end{cases} \tag{25}$$

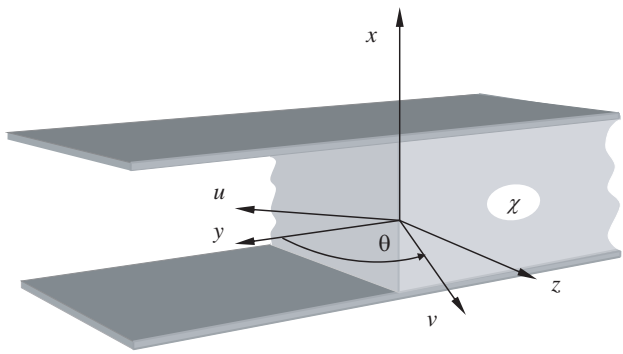

Figure 4. Step discontinuity in a chiral parallel-plate waveguide and the corresponding coordinate systems (x, y, z) and (x, u, v).

After replacing (25) in (24), one gets, for the incident wave,

$$\begin{cases} E_x^i = E_x \exp\left[-j\left(qy + kz\right)\right] \\ E_y^i = \left[\sin\theta E_u + \cos\theta E_v\right] \exp\left[-j\left(qy + kz\right)\right] \\ E_z^i = \left[-\cos\theta E_u + \sin\theta E_v\right] \exp\left[-j\left(qy + kz\right)\right] \\ H_x^i = H_x \exp\left[-j\left(qy + kz\right)\right] \\ H_y^i = \left[\sin\theta H_u + \cos\theta H_v\right] \exp\left[-j\left(qy + kz\right)\right] \\ H_z^i = \left[-\cos\theta H_u + \sin\theta H_v\right] \exp\left[-j\left(qy + kz\right)\right] \end{cases} \tag{26}$$

Similarly, for the reflected wave, one has

$$\begin{cases} E_x^r = E_x \exp\left[-j\left(-qy + kz\right)\right] \\ E_y^r = \left[\sin\theta E_u - \cos\theta E_v\right] \exp\left[-j\left(-qy + kz\right)\right] \\ E_z^r = \left[\cos\theta E_u + \sin\theta E_v\right] \exp\left[-j\left(-qy + kz\right)\right] \\ H_x^r = H_x \exp\left[-j\left(-qy + kz\right)\right] \\ H_y^r = \left[\sin\theta H_u - \cos\theta H_v\right] \exp\left[-j\left(-qy + kz\right)\right] \\ H_z^r = \left[\cos\theta H_u + \sin\theta H_v\right] \exp\left[-j\left(-qy + kz\right)\right] \end{cases} \tag{27}$$

while, for a transmitted wave,

$$\begin{cases} E_x^t = \bar{E}_x \exp\left[-j\left(\bar{q}y + kz\right)\right] \\ E_y^t = \left[\sin\bar{\theta}\bar{E}_u + \cos\bar{\theta}\bar{E}_v\right] \exp\left[-j\left(\bar{q}y + kz\right)\right] \\ E_z^t = \left[-\cos\bar{\theta}\bar{E}_u + \sin\bar{\theta}\bar{E}_v\right] \exp\left[-j\left(\bar{q}y + kz\right)\right] \\ H_x^t = \bar{H}_x \exp\left[-j\left(\bar{q}y + kz\right)\right] \\ H_y^i = \left[\sin\bar{\theta}\bar{H}_u + \cos\bar{\theta}\bar{H}_v\right] \exp\left[-j\left(\bar{q}y + kz\right)\right] \\ H_z^t = \left[-\cos\bar{\theta}\bar{H}_u + \sin\bar{\theta}\bar{H}_v\right] \exp\left[-j\left(\bar{q}y + kz\right)\right] \end{cases} \tag{28}$$

where the variables with a bar stand for the air parallel-plate waveguide, and $\bar{\theta}$ is the propagating angle for the transmitted wave.

In general, there may be a set of elementary modes propagating in each of the two sides of the step. Therefore, the total fields must be written as the modal superposition of the individual fields of each mode, according to

$$\begin{cases} E_x^i = \sum\limits_{n=1}^{\infty} a_n E_{x_n} \exp\left[-j\left(q_n y + kz\right)\right] \\ E_x^r = \sum\limits_{n=1}^{\infty} b_n E_{x_n} \exp\left[-j\left(-q_n y + kz\right)\right] \\ E_x^t = \sum\limits_{p=1}^{\infty} c_p \bar{E}_{x_p} \exp\left[-j\left(\bar{q}_n y + kz\right)\right] \end{cases} \tag{29}$$

$$\begin{cases} H_x^i = \sum\limits_{n=1}^{\infty} a_n H_{x_n} \exp\left[-j\left(q_n y + kz\right)\right] \\ H_x^r = \sum\limits_{n=1}^{\infty} b_n H_{x_n} \exp\left[-j\left(-q_n y + kz\right)\right] \\ H_x^t = \sum\limits_{p=1}^{\infty} c_p \bar{H}_{x_p} \exp\left[-j\left(\bar{q}_n y + kz\right)\right] \end{cases} \tag{30}$$

$$\begin{cases} E_z^i = \sum\limits_{n=1}^{\infty} a_n \left[-\cos\theta_n E_{u_n} + \sin\theta_n E_{v_n}\right] \exp\left[-j\left(q_n y + kz\right)\right] \\ E_z^r = \sum\limits_{n=1}^{\infty} b_n \left[\cos\theta_n E_{u_n} + \sin\theta_n E_{v_n}\right] \exp\left[-j\left(-q_n y + kz\right)\right] \\ E_z^t = \sum\limits_{p=1}^{\infty} c_p \left[-\cos\bar{\theta}_p \bar{E}_{u_p} + \sin\bar{\theta}_p \bar{E}_{v_p}\right] \exp\left[-j\left(\bar{q}_n y + kz\right)\right] \end{cases} \tag{31}$$

and

$$\begin{cases} H_z^i = \sum\limits_{n=1}^{\infty} a_n \left[-\cos\theta_n H_{u_n} + \sin\theta_n H_{v_n}\right] \exp\left[-j\left(q_n y + kz\right)\right] \\ H_z^r = \sum\limits_{n=1}^{\infty} b_n \left[\cos\theta_n H_{u_n} + \sin\theta_n H_{v_n}\right] \exp\left[-j\left(-q_n y + kz\right)\right] \\ H_z^t = \sum\limits_{p=1}^{\infty} c_p \left[-\cos\bar{\theta}_p \bar{H}_{u_p} + \sin\bar{\theta}_p \bar{H}_{v_p}\right] \exp\left[-j\left(\bar{q}_n y + kz\right)\right] \end{cases} \tag{32}$$

The boundary conditions at $y = 0$ may be written in the following form:

$$E_x^i(0) + E_x^r(0) = E_x^t(0) \tag{33}$$

$$H_x^i(0) + H_x^r(0) = H_x^t(0) \tag{34}$$

$$E_z^i(0) + E_z^r(0) = E_z^t(0) \tag{35}$$

$$H_z^i(0) + H_z^r(0) = H_z^t(0) \tag{36}$$

Replacing (29) in (33) one gets

$$\sum_{n=1}^{\infty} (a_n + b_n) E_{x_n} = \sum_{p=1}^{\infty} c_p \bar{E}_{x_p} \tag{37}$$

On the other hand, replacing (30) in (34) one has

$$\sum_{n=1}^{\infty} (a_n + b_n) H_{x_n} = \sum_{p=1}^{\infty} c_p \bar{H}_{x_p} \tag{38}$$

Replacing (31) in (35) one has

$$\begin{aligned} &-\sum_{n=1}^{\infty} (a_n - b_n) \cos\theta_n E_{u_n} + \sum_{n=1}^{\infty} (a_n + b_n) \sin\theta_n E_{v_n} \\ &= \sum_{p=1}^{\infty} c_p \left[-\cos\bar{\theta}_p \bar{E}_{u_p} + \sin\bar{\theta}_p \bar{E}_{v_p}\right] \end{aligned} \tag{39}$$

Finally, after replacing (32) in (36), one gets

$$-\sum_{n=1}^{\infty}(a_n - b_n)\cos\theta_n H_{u_n} + \sum_{n=1}^{\infty}(a_n + b_n)\sin\theta_n H_{v_n}$$
$$= \sum_{p=1}^{\infty} c_p \left[-\cos\bar{\theta}_p \bar{H}_{u_p} + \sin\bar{\theta}_p \bar{H}_{v_n}\right] \tag{40}$$

3.2. Orthogonality Relations

Introducing the following vector inner product

$$\langle \mathbf{f}, \mathbf{g} \rangle = \int_{-b}^{b} (f_1 g_1 + f_2 g_2) dx. \tag{41}$$

the orthogonality relations for the hybrid modes can be written in the following form

$$O_{pm} = \langle \mathbf{W} \cdot \boldsymbol{\varphi}_m, \boldsymbol{\varphi}_n \rangle = \delta_{mn} \tag{42}$$

where δ_{mn} stands for the Kronecker delta,

$$\phi_m = \begin{bmatrix} E_{u_m} & H_{u_m} \end{bmatrix}^T \tag{43}$$

and

$$\mathbf{W} = \frac{1}{\Delta} \begin{bmatrix} \varepsilon & j\chi \\ j\chi & -\mu \end{bmatrix}. \tag{44}$$

On the other hand,

$$\boldsymbol{\psi} = -\beta \mathbf{W} \cdot \boldsymbol{\varphi} \tag{45}$$

with

$$\boldsymbol{\psi} = \begin{bmatrix} H_x & E_x \end{bmatrix}^T. \tag{46}$$

Therefore,

$$O_{pm} = -\beta_p \langle \mathbf{W} \cdot \boldsymbol{\varphi}_p, \boldsymbol{\varphi}_m \rangle = \int_{-b}^{b} (H_{x_p} E_{u_m} + E_{x_p} H_{u_m}) dx = -\beta_p \delta_{pm}. \tag{47}$$

3.3. Mode Matching

Multiplying Equation (38) by $\bar{E}_{u_m}(x)$ and Equation (37) by $\bar{H}_{u_m}(x)$, adding and integrating between $-b$ and $+b$, and using the orthogonality

relations, one can get the amplitude coefficients c_m of the transmitted waves

$$c_m = -\frac{1}{\bar{\beta}_m} \sum_{n=1}^{\infty} (a_n + b_n) P_{nm} \tag{48}$$

where

$$P_{nm} = -\beta_n \left\langle \mathbf{W} \cdot \boldsymbol{\varphi}_n, \bar{\boldsymbol{\varphi}}_m \right\rangle = \int_{-b}^{b} (H_{x_n} \bar{E}_{u_m} + E_{x_n} \bar{H}_{u_m}) dx \tag{49}$$

On the other hand, multiplying Equation (39) by $\bar{H}_{x_m}(x)$ and Equation (40) by $\bar{E}_{x_m}(x)$, adding and integrating between $-b$ and $+b$, and using the orthogonality relation one can get

$$\begin{aligned} &-\sum_{n=1}^{\infty} (a_n - b_n) \cos\theta_n Q_{mn} + \sum_{n=1}^{\infty} (a_n + b_n) \sin\theta_n R_{mn} \\ &= c_m \cos\bar{\theta}_m \bar{\beta}_m + \sum_{p=1}^{\infty} c_p \sin\bar{\theta}_p S_{mp} \end{aligned} \tag{50}$$

where

$$Q_{mn} = -\bar{\beta}_m \left\langle \bar{\mathbf{W}} \cdot \bar{\boldsymbol{\varphi}}_m, \boldsymbol{\varphi}_n \right\rangle = \int_{-b}^{b} (\bar{H}_{x_m} E_{u_n} + \bar{E}_{x_m} H_{u_n}) dx \tag{51}$$

and

$$R_{mn} = -\bar{\beta}_m \left\langle \bar{\mathbf{W}} \cdot \bar{\boldsymbol{\varphi}}_m, \boldsymbol{\kappa}_n \right\rangle = \int_{-b}^{b} (\bar{H}_{x_m} E_{v_n} + \bar{E}_{x_m} H_{v_n}) dx \tag{52}$$

$$S_{mp} = -\bar{\beta}_m \left\langle \bar{\mathbf{W}} \cdot \bar{\boldsymbol{\varphi}}_m, \bar{\boldsymbol{\kappa}}_p \right\rangle = \int_{-b}^{b} (\bar{H}_{x_m} \bar{E}_{v_p} + \bar{E}_{x_m} \bar{H}_{v_p}) dx \tag{53}$$

with $\boldsymbol{\kappa} = \begin{bmatrix} E_v & H_v \end{bmatrix}^T$. The bi-orthogonality relations (49) and (51) are derived in Appendix B. Finally, replacing (48) in (50) one has

$$\begin{aligned} &\sum_{n=1}^{\infty} a_n \left(\cos\theta_n Q_{mn} - \sin\theta_n R_{mn} - \cos\bar{\theta}_m P_{nm} - \sum_{p=1}^{\infty} \frac{1}{\bar{\beta}_p} \sin\bar{\theta}_p P_{np} S_{mp} \right) \\ &= \sum_{n=1}^{\infty} b_n \left(\cos\theta_n Q_{mn} + \sin\theta_n R_{mn} + \cos\bar{\theta}_m P_{nm} + \sum_{p=1}^{\infty} \frac{1}{\bar{\beta}_p} \sin\bar{\theta}_p P_{np} S_{mp} \right) \end{aligned} \tag{54}$$

Defining

$$\mathbf{a} = [\ a_1,\ \ a_2,\ \ \ldots,\ \ a_n,\ \ \ldots\ ]^{\mathrm{T}} \tag{55}$$

$$\mathbf{b} = [\ b_1,\ \ b_2,\ \ \ldots,\ \ b_n,\ \ \ldots\ ]^{\mathrm{T}} \tag{56}$$

Equation (54) can be written in the following matrix form

$$\mathbf{A} \cdot \mathbf{a} = \mathbf{B} \cdot \mathbf{b}, \tag{57}$$

where

$$A_{mn} = \cos\theta_n Q_{mn} - \sin\theta_n R_{mn} - \cos\bar{\theta}_m P_{nm} - \sum_{p=1}^{\infty} \frac{1}{\bar{\beta}_p} \sin\bar{\theta}_p P_{np} S_{mp} \tag{58}$$

$$B_{mn} = \cos\theta_n Q_{mn} + \sin\theta_n R_{mn} + \cos\bar{\theta}_m P_{nm} + \sum_{p=1}^{\infty} \frac{1}{\bar{\beta}_p} \sin\bar{\theta}_p P_{np} S_{mp} \tag{59}$$

Finally, Equation (57) may be rewritten as

$$(\mathbf{C} + \mathbf{D}) \cdot \mathbf{a} = (\mathbf{C} - \mathbf{D}) \cdot \mathbf{b}, \tag{60}$$

where

$$C_{mn} = \cos\theta_n Q_{mn} \tag{61}$$

$$D_{mn} = -\sin\theta_n R_{mn} - \cos\bar{\theta}_m P_{nm} - \sum_{p=1}^{\infty} \frac{1}{\bar{\beta}_p} \sin\bar{\theta}_p P_{np} S_{mp} \tag{62}$$

4. THE CHIRAL H-GUIDE

4.1. Transverse Resonance

Referring to the waveguide depicted in Fig. 1, the plane $y = 0$ is a geometrical symmetry plane. Therefore, one has only to analyze the region $y \geq 0$. In fact, relatively to y, the supermodes can be divided into even and odd modes.

In that case, for the even modes, the boundary conditions at $y = 0$ are

$$H_x^i(0) + H_x^r(0) = 0 \tag{63}$$

$$H_z^i(0) + H_z^r(0) = 0, \tag{64}$$

whilst, for the odd modes they are written as

$$E_x^i(0) + E_x^r(0) = 0 \tag{65}$$

$$E_z^i(0) + E_z^r(0) = 0. \tag{66}$$

From (63) and (64), one has

$$\mathbf{a} = -\mathbf{L} \cdot \mathbf{b} \tag{67}$$

where

$$\mathbf{L} = \text{diag}(\ e^{-j2q_1 l},\ e^{-j2q_2 l},\ \ldots,\ e^{-j2q_n l},\ \ldots\ ) \tag{68}$$

On the other hand, from (65) and (66), one has

$$\mathbf{a} = \mathbf{L} \cdot \mathbf{b} \tag{69}$$

Therefore, it is possible to write

$$\mathbf{a} = \overleftarrow{\mathbf{\Gamma}} \cdot \mathbf{b} \tag{70}$$

where

$$\overleftarrow{\mathbf{\Gamma}} = \Gamma\, \mathbf{L} \tag{71}$$

and $\Gamma = +1$ for the even modes and $\Gamma = -1$ for the odd modes. Replacing (67) in (57) it is possible to get

$$(\mathbf{A} \cdot \overleftarrow{\mathbf{\Gamma}} - \mathbf{B}) \cdot \mathbf{b} = \mathbf{0}, \tag{72}$$

or, from (60),

$$\left[\mathbf{C}\ (\overleftarrow{\mathbf{\Gamma}} - \mathbf{I}) + \mathbf{D}\ (\overleftarrow{\mathbf{\Gamma}} + \mathbf{I})\right] \cdot \mathbf{b} = \mathbf{0}, \tag{73}$$

where, again, $\mathbf{I}$ stands for the unit matrix. Non-trivial solutions of (73) are only possible when

$$\det\left[\mathbf{I} + \frac{\mathbf{D}\ (\overleftarrow{\mathbf{\Gamma}} + \mathbf{I})}{\mathbf{C}\ (\overleftarrow{\mathbf{\Gamma}} - \mathbf{I})}\right] = 0. \tag{74}$$

Equation (74) is the modal equation of the waveguide in Fig. 1, which was derived using the transverse resonance method.

4.2. Numerical Results

In this section, some numerical results for the chiral H-guide, depicted in Fig. 1, are presented. These results have been obtained using the formalism developed in the previous sections. All the elementary surface modes in each region, propagating above cutoff, have been included in the analysis.

The dispersion diagram for the modes in a chiral-parallel plate waveguide and for an empty parallel-plate waveguide are both depicted in Fig. 5. For example, using $b/\lambda = 0.3$, the vertical line drawn in this diagram dictates the number of modes propagating above cutoff and the values for their longitudinal wavenumbers. These elementary modes are necessary for the analysis of the chiral H-guide.

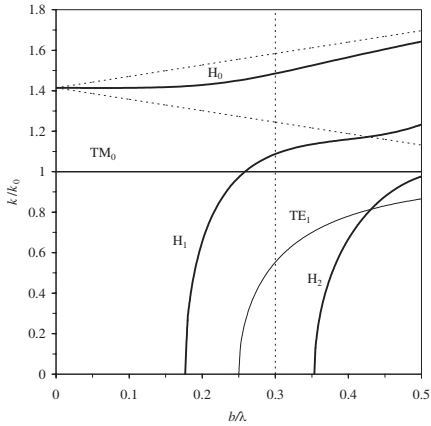

Figure 5. Dispersion diagram for the even modes of a chiral parallel-plate waveguide, with $\varepsilon = 2$, $\mu = 1$, $b = 1\,\mathrm{mm}$, and $g = 10^{-21}\,\mathrm{s^2m^{-1}}$ (thick lines). The thin lines are for the empty parallel-plate waveguide.

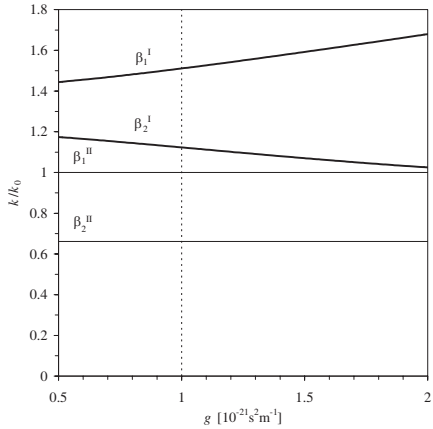

Figure 6. Variation of the longitudinal wavenumbers with the girotropy parameter, when $\varepsilon = 2$, $\mu = 1$, $b = 1\,\mathrm{mm}$, and $b/\lambda = 0.3$ (thick lines). The thin lines are for the empty parallel-plate waveguide.

The variation of the longitudinal wavenumbers of these modes with the girotropy parameter is depicted in Fig. 6. Again, for a given value of the girotropy parameter, e.g., $g = 10^{-21}\,\mathrm{s^2m^{-1}}$, the vertical line drawn in this diagram gives the values for the longitudinal wavenumbers of these modes.

The operational diagram for a chiral H-guide is depicted in Fig. 7. The vertical dashed line gives the cutoff values for the slab half-width, telling how many modes are propagating in the structure for a given set of parameters. The modes are termed H_n, meaning that they are all hybrid, with n being the order of the mode and expressing the number of maximums in the inner region. As was already pointed out, due to the waveguide spatial symmetry relatively to the central plane $y = 0$, every propagating mode has either even or odd symmetry.

The effect of the slab width in the value of the longitudinal wavenumber for the first propagating modes is illustrated in Fig. 8. Results for the case of an H-guide with vanishing chirality (i.e., using a conventional dielectric) are also depicted to put in evidence the differences between the chiral and the achiral cases. As was expected, for the chiral case, there is also a fundamental mode with no cutoff, while mode coupling between some of the modal curves can be easily identified.

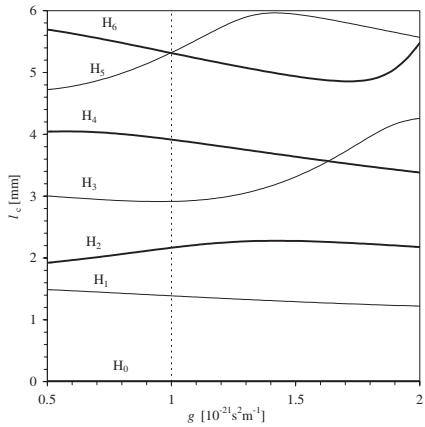

Figure 7. Operational diagram for a chiral H-guide with $b = 1\,\text{mm}$, when $\varepsilon = 2$, $\mu = 1$, and $f = 100\,\text{GHz}$.

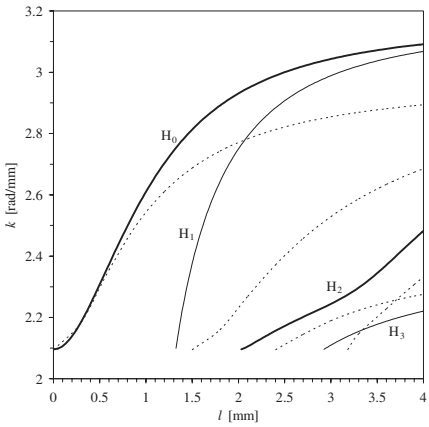

Figure 8. Effect of the slab width on the H-guide performance for $g = 10^{-21}\,\text{s}^2\text{m}^{-1}$ (dashed lines are for vanishing chirality).

5. CONCLUSIONS

We have proposed a semi-analytical method based on a building-block approach, suitable to analyze 3D chiral waveguides with rectangular geometry. So far, this type of waveguides had only been analyzed through the use of fully numerical methods. In this paper, the conventional mode matching technique and the usual transverse resonance method have been generalized to be applied to the hybrid guided modes of chiral waveguides with rectangular geometry. The proposed method was successfully applied to the analysis of a chiral H-guide. A full parametric study was presented for a chiral H-guide operating at a fixed frequency. The numerical results show that chirality may provide an extra degree of freedom useful for the design of new devices.

ACKNOWLEDGMENT

This work was partially funded by FCT (Fundação para a Ciência e a Tecnologia), Portugal.

APPENDIX A. FIELD COMPONENTS FOR THE EVEN HYBRID MODES OF THE CHIRAL PARALLEL-PLATE WAVEGUIDE

For a chiral parallel-plate waveguide, one has

$$\begin{cases} E_y = A\left[\cos(h_+x) + Q\cos(h_-x)\right] \\ H_y = jY_cA\left[\cos(h_+x) - Q\cos(h_-x)\right] \end{cases} \tag{A1}$$

$$\begin{cases} E_x = A\frac{jY_ck}{\omega\varepsilon_0}\left[\frac{1}{\varepsilon_+}\cos(h_+x) - \frac{Q}{\varepsilon_-}\cos(h_-x)\right] \\ H_x = -A\frac{k}{\omega\mu_0}\left[\frac{1}{\mu_+}\cos(h_+x) + \frac{Q}{\mu_-}\cos(h_-x)\right] \end{cases} \tag{A2}$$

$$\begin{cases} E_z = A\frac{Y_c}{\omega\varepsilon_0}\left[-\frac{h_+}{\varepsilon_+}\sin(h_+x) + \frac{h_-Q}{\varepsilon_-}\sin(h_-x)\right] \\ H_z = A\frac{j}{\omega\mu_0}\left[-\frac{h_+}{\mu_+}\sin(h_+x) - \frac{h_-Q}{\mu_-}\sin(h_-x)\right] \end{cases} \tag{A3}$$

The case of an air parallel plate waveguide can be recovered by making $\varepsilon_+ = \varepsilon_- = 1$, $\mu_+ = \mu_- = 1$, $Y_c = Y_0$ and $h_+ = h_- = h_m = m\pi/(2b)$, with $m = 1, 2, 3\ldots$. The fundamental mode TM_0, with no cutoff frequency, is obtained for $m = 0$. For TE modes one has $Q = 1$ while for TM modes $Q = -1$.

APPENDIX B. BI-ORTHOGONALITY RELATIONS

The bi-orthogonality relation P_{nm} between the modes of each region is defined as

$$P_{nm} = -\beta_n \left\langle \mathbf{W}\cdot\boldsymbol{\varphi}_n, \bar{\boldsymbol{\varphi}}_m \right\rangle = \int_{-b}^{b} (H_{x_n}\bar{E}_{u_m} + E_{x_n}\bar{H}_{u_m})dx \tag{B1}$$

or

$$\begin{aligned} P_{nm} \;=\; & -A_nA_m\frac{k_n}{\omega}\left[\left(\frac{1}{\mu_+\mu_0} + \frac{Y_cY_0}{\varepsilon_+\varepsilon_0}\right)\int_{-b}^{b}\cos(h_{+_n}x)\cos(h_mx)dx\right. \\ & +Q_m\left(\frac{1}{\mu_+\mu_0} - \frac{Y_cY_0}{\varepsilon_+\varepsilon_0}\right)\int_{-b}^{b}\cos(h_{+_n}x)\cos(h_mx)dx \\ & +Q_n\left(\frac{1}{\mu_-\mu_0} - \frac{Y_cY_0}{\varepsilon_-\varepsilon_0}\right)\int_{-b}^{b}\cos(h_{-_n}x)\cos(h_mx)dx \\ & \left.+\,Q_nQ_m\left(\frac{1}{\mu_-\mu_0} + \frac{Y_cY_0}{\varepsilon_-\varepsilon_0}\right)\int_{-b}^{b}\cos(h_{-_n}x)\cos(h_mx)dx\right\} \end{aligned} \tag{B2}$$

Finally,

$$\begin{aligned} P_{nm} &= -\frac{2k_n}{\omega}\left\{\frac{\frac{1+Q_m}{\mu_0\mu_+}+\frac{1-Q_m}{\varepsilon_+\varepsilon_0}Y_cY_0}{h_{+_n}^2-h_m^2}\right. \\ &\quad [h_{+_n}\sin(h_{+_n}b)\cos(h_mb)-h_m\cos(h_{-_n}b)\sin(h_mb)] \\ &\quad +\frac{\frac{1+Q_m}{\mu_0\mu_-}-\frac{1-Q_m}{\varepsilon_-\varepsilon_0}Y_cY_0}{h_{-_n}^2-h_m^2}\,Q_n \\ &\quad \left.[h_{-_n}\sin(h_{-_n}b)\cos(h_mb)-h_m\cos(h_{-_n}b)\sin(h_mb)]\right\} \quad \text{(B3)} \end{aligned}$$

The bi-orthogonality relation Q_{mn} between the modes of each region is defined as

$$Q_{mn} = -\bar{\beta}_m\left\langle \bar{\mathbf{W}}\cdot\bar{\boldsymbol{\varphi}}_m, \boldsymbol{\varphi}_n\right\rangle = \int_{-b}^{b}(\bar{H}_{x_m}E_{u_n}+\bar{E}_{x_m}H_{u_n})dx \quad \text{(B4)}$$

or

$$\begin{aligned} Q_{mn} &= -A_mA_n\frac{k_m}{\omega}\left[\left(\frac{1}{\mu_0}+\frac{Y_cY_0}{\varepsilon_0}\right)\int_{-b}^{b}\cos(h_{+_m}x)\cos(h_nx)dx\right. \\ &\quad +Q_n\left(\frac{1}{\mu_0}-\frac{Y_cY_0}{\varepsilon_0}\right)\int_{-b}^{b}\cos(h_{+_m}x)\cos(h_nx)dx \\ &\quad +Q_m\left(\frac{1}{\mu_0}-\frac{Y_cY_0}{\varepsilon_0}\right)\int_{-b}^{b}\cos(h_{-_m}x)\cos(h_nx)dx \\ &\quad \left.+Q_mQ_n\left(\frac{1}{\mu_0}+\frac{Y_cY_0}{\varepsilon_0}\right)\int_{-b}^{b}\cos(h_{-_m}x)\cos(h_nx)dx\right\} \quad \text{(B5)} \end{aligned}$$

Finally,

$$\begin{aligned} Q_{mn} &= -\frac{2k_m}{\omega}\left\{\frac{\frac{1+Q_n}{\mu_0}+\frac{1-Q_n}{\varepsilon_0}Y_cY_0}{h_{+_m}^2-h_n^2}\right. \\ &\quad [h_{+_m}\sin(h_{+_m}b)\cos(h_nb)-h_n\cos(h_{-_m}b)\sin(h_nb)] \\ &\quad +\frac{\frac{1+Q_n}{\mu_0}-\frac{1-Q_n}{\varepsilon_0}Y_cY_0}{h_{-_m}^2-h_n^2}\,Q_m \\ &\quad \left.[h_{-_m}\sin(h_{-_m}b)\cos(h_nb)-h_n\cos(h_{-_m}b)\sin(h_nb)]\right\} \quad \text{(B6)} \end{aligned}$$

REFERENCES

1. Cory, H., "Chiral devices — An overview of canonical problems," *Journal of Electromagnetic Waves and Applications*, Vol. 9, No. 5–6, 805–829, 1995.
2. Svedin, J. A. M., "Finite-element analysis of chirowaveguides," *Electronics Lett.*, Vol. 26, No. 13, 928–929, June 1990.
3. Pelet, P. and N. Engheta, "Modal analysis for rectangular chirowaveguides with metallic walls using the finite-difference method," *Journal of Electromagnetic Waves and Applications*, Vol. 6, No. 9, 1277–1285, 1992.
4. Cory, H., "Wave propagation along a closed rectangular chirowaveguide," *Microwave Opt. Technol. Lett.*, Vol. 6, No. 14, 797–800, November 1993.
5. Paiva, C. R. and A. M. Barbosa, "A method for the analysis of biisotropic planar waveguides — Application to a grounded chiroslabguide," *Electromagnetics*, Vol. 11, No. 1, 209–221, March 1991.
6. Engheta, N. and P. Pelet, "Modes in chirowaveguides," *Optics Lett.*, Vol. 14, No. 11, 593–595, June 1989.
7. Pelet, P. and N. Engheta, "The theory of chirowaveguides," *IEEE Trans. Antennas Propagat.* Vol. 38, No. 1, 90–98, 1990.
8. Mahamoud, S. F., "On mode bifurcation in chirowaveguides with perfect electric walls," *Journal of Electromagnetic Waves and Applications*, Vol. 6, No. 10, 1381–1392, 1992.
9. Toscano, A. and L. Vegni, "Effects of chirality admittance on the propagating modes in a parallel-plate waveguide partially filled with a chiral slab," *Microwave Opt. Technol. Lett.*, Vol. 6, No 14, 806–809, November 1993.
10. Cory, H. and S. Waxman, "Wave propagation along a fully or a partially loaded parallel plate chirowaveguides," *IEE Proc.-Microw. Antennas Propag.*, Vol. 141, No. 4, 299–306, August 1994.
11. Gómez, A., A. Lakhtakia, J. Margineda, G. J. Molina-Cuberos, M. J. Núñez, J. A. S. Ipiña, A. Vegas, and M. A. Solano, "Full-wave hybrid technique for 3-D isotropic-chiral-material discontinuities in rectangular waveguides: Theory and experiment," *IEEE Trans. Microwave Theory Tech.*, Vol. 56, 2815–2825, 2008.
12. Goméz, A., A. Vegas, and M. A. Solano, "A brief discussion on the different formulations of the coupled mode method in chiral media: Application to the parallel-plate chirowaveguide," *Microwave Opt. Technol. Lett.*, Vol. 42, No. 3, 181–185, August 2004.

13. Herman, W. N., "Polarization eccentricity of the transverse field for modes in chiral core planar waveguides," *J. Opt. Soc. Am. A*, Vol. 18, No. 11, 2806–2818, 2001.
14. Bahar, E., "Mueller matrices for waves reflected and transmitted through chiral materials: Waveguide modal solutions and applications," *J. Opt. Soc. Am. B*, Vol. 24, No. 7, 1610–1619, 2007.
15. César, A. and R. Souza, "Uniaxial anisotropy effect on the non-radiative dielectric (NRD) waveguide performance," *PIERS Proceedings*, Vol. 1, 207, Hong Kong, January 1997.
16. César, A. and R. Souza, "Full-wave analysis of a transversely magnetized ferrite nonradiative dielectric waveguide," *IEEE Trans. Microwave Theory Tech.*, Vol. 41, 647–651, April 1993.
17. Topa, A. L., C. R. Paiva, and A. M. Barbosa, "Full-wave analysis of a nonradiative dielectric waveguide with a pseudochiral omega slab," *IEEE Trans. Microwave Theory Tech.*, Vol. 46, 1263–1269, September 1998.
18. Topa, A. L., C. R. Paiva, and A. M. Barbosa, "Novel propagation features of double negative H-guides and H-guide couplers," *Microwave Opt. Technol. Lett.*, Vol. 47, No. 2, 185–190, October 2005.
19. Topa, A. L., C. R. Paiva, and A. M. Barbosa, "Electromagnetic wave propagation in omega waveguides: Discrete complex modes and application to a ridge waveguide," *Progress In Electromagnetic Research*, PIER 49, 309–331, 2004.
20. Topa, A. L., C. R. Paiva, and A. M. Barbosa, "Guidance and leakage behavior of uniaxial ridge waveguides," *Journal of Electromagnetic Waves and Applications*, Vol. 23, No. 13, 1675–1684, 2009.
21. Oliner, A. A., S.-T. Peng, T.-H. Hsu, and A. Sanchez, "Guidance and leakage properties of a class of open dielectric waveguides: Part II — New physical effects," *IEEE Trans. Microwave Theory Tech.*, Vol. 29, 855–869, 1981.
22. Condon, E. U., "Theory of optical rotatory power," *Rev. Mod. Phys.*, Vol. 9, 432–457, 1937.
23. Lakhtakia, A., V. K. Varadan, and V. V. Varadan, "Bohren's decomposition," *Time-Harmonic Electromagnetic Fields in Chiral Media*, Vol. 335, 30–33, Edited by A. Lakhtakia, V. K. Varadan, and V. V. Varadan, Springer, Lecture Notes in Physics, 1989.